analytical chemistry

pubs.acs.org/ac Article

Combination of IM-Based Approaches to Unravel the Coexistence of Two Conformers on a Therapeutic Multispecific mAb

Evolène Deslignière, Simon Ollivier, Anthony Ehkirch, Armelle Martelet, David Ropartz, Nelly Lechat, Oscar Hernandez-Alba, Jean-Michel Menet, Séverine Clavier, Hélène Rogniaux, Bruno Genet, and Sarah Cianférani*

Cite This: *Anal. Chem.* 2022, 94, 7981−7989 Read Online

ACCESS | Metrics & More | Article Recommendations | Supporting Information

ABSTRACT: Multispecific antibodies, which target multiple antigens at once, are emerging as promising therapeutic entities to offer more effective treatment than conventional monoclonal antibodies (mAbs). However, these highly complex mAb formats pose significant analytical challenges. We report here on the characterization of a trispecific antibody (tsAb), which presents two isomeric forms clearly separated and identified with size exclusion chromatography coupled to native mass spectrometry (SEC-nMS). Previous studies showed that these isomers might originate from a proline *cis*/*trans* isomerization in one Fab subunit of the tsAb. We combined several innovative ion mobility (IM)-based approaches to confirm the isomeric nature of the two species and to gain new insights into the conformational landscape of both isomers. Preliminary SEC-nIM-MS measurements performed on a low IM resolution instrument provided the first hints of the coexistence of different conformers, while complementary collision-induced unfolding (CIU) experiments evidenced distinct gas-phase unfolding behaviors upon activation for the two isomers. As subtle conformational differences remained poorly resolved on our early generation IM platform, we performed high-resolution cyclic IM (cIM-MS) to unambiguously conclude on the coexistence of two conformers. The *cis*/*trans* equilibrium was further tackled by exploiting the IM^n slicing capabilities of the cIM-MS instrument. Altogether, our results clearly illustrate the benefits of combining state-of-the-art nMS and IM-MS approaches to address challenging issues encountered in biopharma. As engineered antibody constructs become increasingly sophisticated, CIU and cIM-MS methodologies undoubtedly have the potential to integrate the drug development analytical toolbox to achieve in-depth conformational characterization of these products.

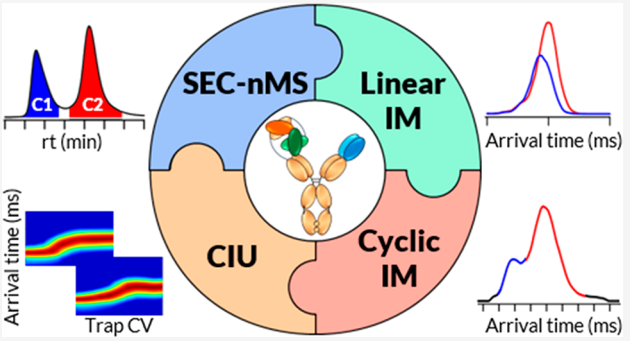

INTRODUCTION

Monoclonal antibodies (mAbs) and their related compounds make up the largest class in human therapeutics to treat various diseases. The success of mAbs stems from their high specificity and affinity, long circulating half-lives, ability to induce immune cell effector response and structural versatility. In the last years, advancement in antibody engineering enabled a high diversity of mAb formats ranging from nanobodies to multispecific antibodies.[1,2] Thus, new immunotherapy approaches are emerging with the use of broadly neutralizing human mAbs, which engage multiple therapeutic targets through a single protein.[3−5] These new-generation antibody drugs provide advantages for various therapeutic applications with the reduced expense of administering of single biologic therapy instead of complex combination treatment.

A trispecific antibody (tsAb) was recently developed to confer protection against diverse HIV strains by targeting three independent HIV-1 envelope determinants: the CD4 binding site, the GP41 membrane proximal external region (MPER), and the variable regions 1 and 2 (V1V2) glycan site.[6] The tsAb consists of variable domains from three different mAbs arranged in an immunoglobulin (IgG1) scaffold:[7−10] one classical antigen-binding fragment (Fab) arm (VRC01) and a bispecific crossover dual variable (CODV) domain arm, as displayed in Figure 1. During preclinical development of the tsAb, an unusual two-peak size exclusion chromatography (SEC) profile was reported by Masiero et al., and conducted to a comprehensive characterization of the complex tsAb architecture.[11] The authors used multiple analytical, bioanalytical and computational methods to understand the tsAb heterogeneity. First results revealed a conformational switching

Received: February 26, 2022
Accepted: May 6, 2022
Published: May 23, 2022

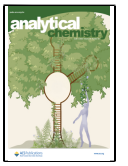

https://doi.org/10.1021/acs.analchem.2c00928
Anal. Chem. 2022, 94, 7981−7989

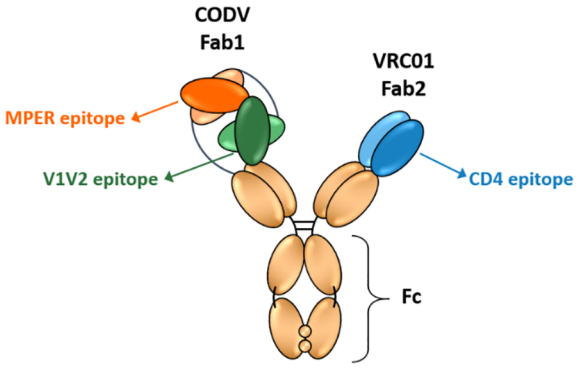

Figure 1. Design of the tsAb. The tsAb consists of variable domains of three different mAbs arranged in an IgG1 scaffold: one classical Fab arm (VRC01), a bispecific crossover dual variable (CODV) domain arm and a fragment crystallizable region (Fc). The variable domains target three independent HIV-1 envelope determinants: the CD4 binding site (blue), the GP41 membrane proximal external region (MPER, orange), and the V1V2 glycan site (green).

in complementarity determining regions (CDR) of the CODV arm due to a specific motif containing proline residues known to induce *cis* and *trans* isomers.[11−14] More specifically, the tyrosine−proline−proline (YPP) motif of the heavy chain CDR3 (variable part targeting MPER epitope) was evidenced as playing a key role in isomerization through the interaction with a histidine residue of the light chain. Guttman et al. also demonstrated that this YPP motif could be responsible for the SEC heterogeneity.[14] For the tsAb studied in the present work, the YPP motif was shown to be essential for the optimal antigen binding as various mutations within the motif led to significant loss of affinity to the target.[11] Besides, previous work demonstrated that, despite a fast sequestration of the more affine *cis* conformer by the antigen and a much slower binding for the *trans* conformer, the potency of the molecule was not impacted by the presence of two isomers due to consequent re-equilibrium of the conformers.[11] Those first studies gave insights into the local conformation of the CDR3 loop, but did not provide information on the global conformation of the two species separated in SEC, and so we aim at characterizing those higher order structures to achieve a comprehensive characterization of the tsAb.

Native mass spectrometry (nMS) and its coupling to ion mobility (nIM-MS) are of utmost interest to probe the native conformational state of proteins in the gas phase and to achieve a multilevel characterization of various mAb formats without extensive sample preparation. nMS and nIM-MS have been promoted for the characterization of biopharmaceuticals thanks to their quite straightforward and rapid workflows, especially through online nondenaturing liquid chromatography couplings.[15−17] IM separates ions based on their size, shape, and charge. Arrival time distributions (ATD) of ions offer structural information and may be converted into rotationally averaged collision cross sections (CCS, also labeled Ω), which reflect gas-phase conformations. However, because of the low IM resolving power ($R \sim 40$ Ω/ΔΩ) of first-generation traveling wave IM spectrometry (TWIMS) instruments, isomeric species with closely related conformations/CCS values often cannot be differentiated using nIM-MS measurements.[18,19] Recent instrumental developments focused on increasing the path length of ions to reach higher IM resolving powers. TWIMS-based structures for lossless ion manipulations with an extended serpentine design (SLIM SUPER) cycle ions through a 13 m path for multiple times and allow the achievement of $R \sim 1860$ for small molecules.[20] In 2019, a new cyclic Q-TWIMS-ToF instrument (cIM-MS) equipped with a cyclic cell placed orthogonally to the axis of the mass spectrometer was commercialized. This design affords higher resolving power through multipass separation, and also offers the unique opportunity to perform IM^n experiments to further explore mobility-separated populations.[21] The cIM-MS platform has proved particularly useful in several studies to differentiate small isomeric analytes,[22,23] with up to $R \sim 750$ Ω/ΔΩ obtained after 100 passes.[21] On the other hand, only few papers have reported the use of high-resolution cIM-MS for the analysis of larger biomolecules (proteins).[24−26] In fact, first studies showed that resolving coexisting conformations of intact proteins in native conditions remains highly challenging because native ions are composed of a continuum of conformers that may be difficult to separate even with enhanced IM resolution.[24] In such cases, alternative strategies can be used to circumvent the lack of IM separation. Collision-induced unfolding (CIU) experiments have arisen as a powerful IM-based approach to distinguish native proteins based on their gas-phase behaviors upon activation in the instrument trap collision cell, located prior to the IM cell which measures the resulting conformational states. This technique appeared to be highly valuable for therapeutic mAb products.[18,19,27−30] In an attempt to automate CIU workflows, Deslignière et al. have proposed a SEC−CIU setup that allows recording CIU fingerprints in a rapid manner.[31]

In this study, we investigate the conformational landscape of the tsAb isomers at both intact and middle-up (i.e., after enzymatic digestion into large subunits[32]) levels by combining innovative SEC-nMS and nIM-based approaches. We illustrate the complementarity of SEC−CIU unfolding patterns and high-resolution IM profiles to address the tsAb heterogeneity and definitely prove the coexistence of two different conformers for the tsAb. We also tackle the *cis*/*trans* isomerization by using slicing IM^n capabilities of the cIM-MS instrument. Our results highlight the synergistic benefits arising from the combined use of SEC-nMS, CIU, and high-resolution IM for a more comprehensive analytical characterization of complex therapeutic formats, such as engineered multispecific antibodies.

MATERIALS AND METHODS

Reagents and Materials. The tsAb and its mutant were obtained from Sanofi (Vitry-sur-Seine, France). Ammonium acetate (A1542) was purchased from Sigma-Aldrich. FabALACTICA (A0-AG1-020) enzymes were obtained from Genovis. Aqueous solutions were prepared using an ultrapure water system (Sartorius, Göttingen, Germany).

Sample Preparation. The enzymatic digestion for middle-up level analyses was performed by incubating one unit of FabALACTICA per microgram of sample overnight at 37 °C. For experiments performed on the cIM-MS instrument (i.e., without SEC upstream of the mass spectrometer), samples were desalted against a 100 mM ammonium acetate solution (pH 6.9) with six cycles of centrifugal microconcentrator (Vivaspin, 30 or 50 kDa cutoffs, Sartorius, Göttingen, Germany). After manual desalting, protein concentration was determined by using an UV-1800 spectrophotometer (Shimadzu Scientific Instruments, Columbia, MD, U.S.A.).

https://doi.org/10.1021/acs.analchem.2c00928
Anal. Chem. 2022, 94, 7981−7989

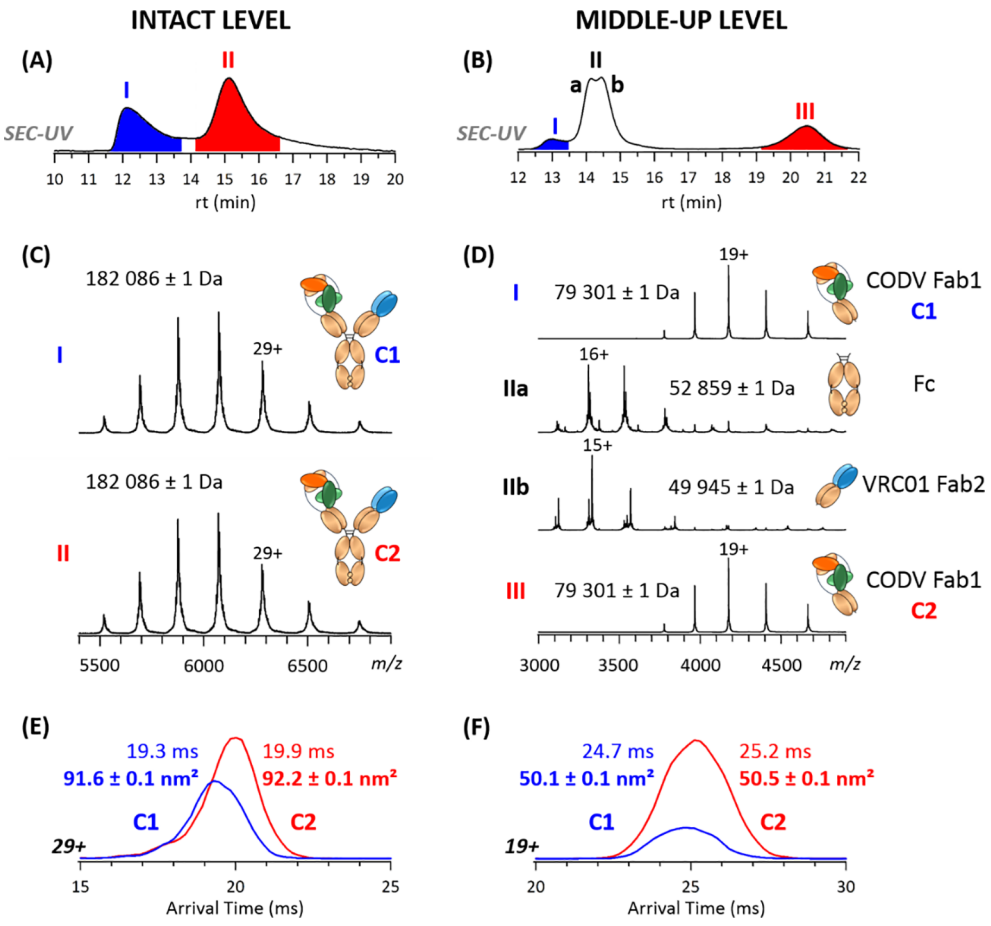

Figure 2. Analysis of the tsAb using online SEC-nMS/nIM-MS. (A, B) SEC-UV chromatograms (280 nm) at intact and middle-up levels. (C, D) nMS spectra of the different species separated with SEC. Extracted ATDs and associated $^{TW}CCS_{N2}$ values for conformers C1 and C2 (E) for the 29+ charge state at intact level and (F) for the 19+ charge state of Fab1 subunits generated after FabALACTICA digestion.

Samples were diluted to a final concentration of 7 μM before cIM-MS analysis.

SEC-nMS Experiments. An Acquity UPLC H-class system (Waters, Milford, MA, U.S.A.) comprising a quaternary solvent manager, a sample manager set to 10 °C, a column oven and a TUV detector operating at 280 and 214 nm, was hyphenated to a Synapt G2 HDMS mass spectrometer (Waters, Wilmslow, U.K.) for online native SEC-(IM)-MS experiments. The SEC column was an Acquity BEH SEC 200 Å, 1.7 μm, 4.6 × 300 mm from Waters. The separation was carried out in isocratic mode with an aqueous mobile phase composed of 100 mM ammonium acetate pH 6.9. For intact level experiments, the flow rate was set to 0.30 mL/min for 5.5 min, and then to 0.10 mL/min for 14.5 min. For middle-up analyses, the following flow rates were used: 0.30 mL/min for 7.5 min; 0.10 mL/min for 15.5 min. The source and desolvation gas temperatures were set to 90 and 450 °C, respectively. The Synapt G2 HDMS was operated in sensitivity mode and positive polarity with a capillary voltage of 3.0 kV. The sample cone voltage and pressure in the interface region were set to 180 V and 6 mbar, respectively. Data were acquired in the m/z range 1000−10000 with a 1.5 s scan time. MS data interpretation was conducted on MassLynx v4.1 (Waters, Manchester, U.K.).

SEC-nIM-MS Experiments. The Synapt G2 HDMS was carefully tuned to achieve a good trade-off between ion separation and TWIMS resolution. The sampling cone was operated at 80 V for the tsAb at middle-up/intact levels and for IM calibrants. The argon flow rate in the trap cell was 5 mL/min. Ions were thermalized in the helium cell (130 mL/min), prior to IM separation which occurred in the pressurized IM cell, under a constant N_2 flow rate of 45 mL/min. For intact level analyses, the IM wave height (WH) and velocity (WV) were set to 40 V and 923 m/s, respectively. At the middle-up level, parameters were tuned to WH = 35 V and WV = 1200 m/s. IM data were calibrated to perform $^{TW}CCS_{N2}$ calculations by measuring external standards (dimeric β-lactoglobulin, avidin, concanavalin A for subunits, and concanavalin A, alcohol dehydrogenase, and pyruvate kinase for intact antibodies) with the same nIM-MS parameters as analytes, as described elsewhere.[33−35] nIM-MS data were collected in triplicate under identical instrumental conditions. Experimental $^{TW}CCS_{N2}$ values for the CODV Fab subunit were compared with theoretical CCS_{N2} obtained with the IMoS v1.10 software.[36] The PDB 5WHZ, which corresponds to the crystal structure of the $YP_{trans}P_{trans}$ isomer,[6] was used as is for theoretical calculations. Calculations were performed with the Exact Hard Sphere Scattering (EHSS) method, which among the three main classes of CCS calculation algorithms[37] offers the best compromise between CCS accuracy and calculation time. The following parameters were used: number of orientations = 3; accommodation coefficient = 0; drift gas = N_2 with corresponding radius = 1.5 Å and polarization = 1.7 Å^3. Averaged theoretical CCS_{N2} values were obtained from six independent calculations performed with different number of

https://doi.org/10.1021/acs.analchem.2c00928
Anal. Chem. 2022, 94, 7981−7989

gas molecules per orientation for each replicate (between 200000 and 400000 molecules).

SEC−CIU Experiments at Intact Level. The SEC−CIU setup used here has been extensively described in another paper.[31] SEC−CIU experiments are performed on the Synapt G2 HDMS by automatically raising trap collision voltages (5 V steps) during the elution of the two intact species via a predefined MS file in MassLynx v4.1 software (Waters, Manchester, UK). The number of scans and scan time for each CV were set to 12 and 1 s, respectively. In order to generate one CIU fingerprint replicate (0−150 V) for both conformational isomers (namely, C1 and C2), SEC−CIU data were collected in eight runs, with eight voltages recorded during each run: 0−15 V/135−150 V for C1/C2 (run 1), 20−35 V/115−130 V for C1/C2 (run 2), and so on. Note that for automated data extraction using CIUSuite 2 v2.2,[38] one run cannot contain two identical CVs, and so different ramps are used for C1/C2. Data sets were collected in triplicate to obtain averaged CIU fingerprints. SEC−CIU data were processed with CIUSuite 2 v2.2.[38] ATDs were smoothed using a Savitsky-Golay algorithm with a window length of 5 and a polynomial order of 2. CIU50 values of conformational transitions were determined using the CIUSuite 2 "Stability Analysis" module. Parameters used for feature detection and CIU50 analysis were as follows: standard mode for feature and CIU50 detections; minimum feature length = 5 steps; feature allowed width = 0.75 ms; drift time spectrum = centroid at maximum value for each CV; transition region padding = 15 V. As differences of unfolding behaviors can be difficult to assess with CIU fingerprints, other representations were exploited: waterfall ATDs were generated with ORIGAMI^{ANALYZE} v1.2.1.4,[39] and intensity weighted mean ATDs were obtained using Benthesikyme.[40]

IM-MS Experiments in the Cyclic Instrument. Acquisitions were performed through direct ESI injection (on a Z-spray ion source equipped with a low flow ESI probe) on a SELECT SERIES Cyclic IMS (Waters, Wilmslow, U.K.). Analyses were recorded at a scanning rate of 1 scan/s, in the m/z range 50−8000 using MassLynx v4.2 (Waters, Wilmslow, U.K.). Samples were analyzed in positive ion mode, with the following parameters: capillary 1.8 kV; sampling cone 80 or 40 V (for intact and middle-up level analyses, respectively); source offset 30 V; source temperature 50 °C; desolvation temperature 250 °C. The pressure in the interface region was 2.6 mbar. cIM experiments were carried out in N60 purity nitrogen (Alphagaz 2, Air Liquide, France), at a pressure of 1.7 mbar. cIM parameters were WH = 45 V and WV = 900 m/s at the intact level, and set to WH = 32 V and WV = 650 m/s for middle-up level analyses. For both intact and middle-up levels, ions were ejected from the cIM racetrack with a forward traveling wave WV = 600 m/s. Note that the voltages in the multifunction array region (that allows to perform fine manipulation of the ion populations during IM and IM^n experiments) were modified to work on native proteins, as described in Table S1.

RESULTS

Characterization of tsAb Conformers at Intact and Middle-up Levels Using SEC-nMS. We first analyzed the tsAb sample by online SEC-nMS for identification of SEC-separated peaks in a fully nondenaturing environment[15] (Figure 2 and Table S2). As already reported, two peaks were observed on the SEC-UV chromatogram and identified as monomers (182086 ± 1 Da) by online nMS (Figure 2A,C), corroborating the hypothesis of conformational isomers further referred to as C1 and C2.[11] This unusual SEC separation might be explained by significant conformational differences between the two monomeric species and/or by chemical interactions with the SEC stationary phase. Adding 10% isopropanol to the mobile phase substantially reduced retention times, especially for the C2 conformer (Figure S1A). Higher concentrations of salt led to an increase of retention times, illustrating the salting-out effect that can occur for hydrophobic mAb products[41] (Figure S1B). These results show that (i) interactions with the stationary phase are mostly hydrophobic and not ionic, and (ii) secondary interactions are not the sole factor driving the separation of C1 and C2 as the two conformers do not coelute even with different mobile phases. As the YPP motif responsible for isomerization is located in the CDR3 of the CODV arm's heavy chain, we next carried out SEC-nMS analysis after FabALACTICA enzymatic digestion. This protease is designed to cleave IgGs above the hinge region, and is thus expected to produce the three following subunits: the Fc, the VRC01 Fab, and the CODV Fab bearing the YPP motif. Three main peaks were detected on the SEC-UV chromatogram (Figure 2B,D), corresponding to four species identified by nMS. Peak I corresponds to Fab1 (79301 ± 1 Da). Peak II contains two partially resolved species, the Fc (IIa, 52859 ± 1 Da) and the Fab2 (IIb, 49945 ± 1 Da) subdomains. Finally, another Fab subunit with exactly the same mass as Fab1 (79301 ± 1 Da) is detected in peak III, which again highlights the coexistence of isomeric Fab1 species bearing the YPP motif. The second Fab1 was eluted significantly later compared to other subunits, which is in part explained by hydrophobic interactions with the stationary phase of the SEC column (Figure S1C,D). Based on SEC-UV areas, relative amounts of C1 and C2 isomers for Fab1 subunits are estimated to be 24 ± 1% and 76 ± 1%. It is noteworthy that a conformer ratio of 37/63 ± 1% for C1/C2 was observed for intact species, which can be explained by the distinct sample buffer pH (i.e., formulation buffer for intact species, enzyme buffer for Fab1 subunits) as Masiero et al. described a pH-sensing conformational equilibrium.[11] To further confirm that the presence of different isomers detected with SEC-nMS is indeed related to the YPP motif, we analyzed an isomerization-free mutant form (AAP motif instead of YPP). At intact level, the mutant tsAb showed only one SEC peak identified as a monomer (181309 ± 1 Da, Figure S2). As expected, a clearly different SEC profile was also obtained after FabALACTICA for the mutant tsAb, with three SEC peaks identified as Fc (52861 ± 1 Da), Fab2 (49365 ± 1 Da) and Fab1 (79110 ± 1 Da) subunits (Figure S2). Altogether, SEC-nMS analyses performed either on intact tsAb or on subunits unambiguously demonstrate that the YPP motif is responsible for the detection of an additional conformer separated on the SEC column.

SEC-nIM-MS Provides First Hints for Conformational Differences between tsAb Isomers. To confirm the existence of the two isomers by an orthogonal biophysical technique, and to determine whether those are conformational isomers, we next performed SEC-nIM-MS experiments to evaluate the conformational landscape of each species. For the 29+ charge state at the intact level, a difference of 0.6 ms was observed between arrival times of both conformers, leading to $^{TW}CCS_{N2}$ values of 91.6 ± 0.1 nm^2 and 92.2 ± 0.1 nm^2 for C1 and C2, respectively (Figure 2E). $\Delta^{TW}CCS_{N2}$ between the two species is comprised between 0.4 and 0.6 nm^2 across all charge

https://doi.org/10.1021/acs.analchem.2c00928
Anal. Chem. 2022, 94, 7981−7989

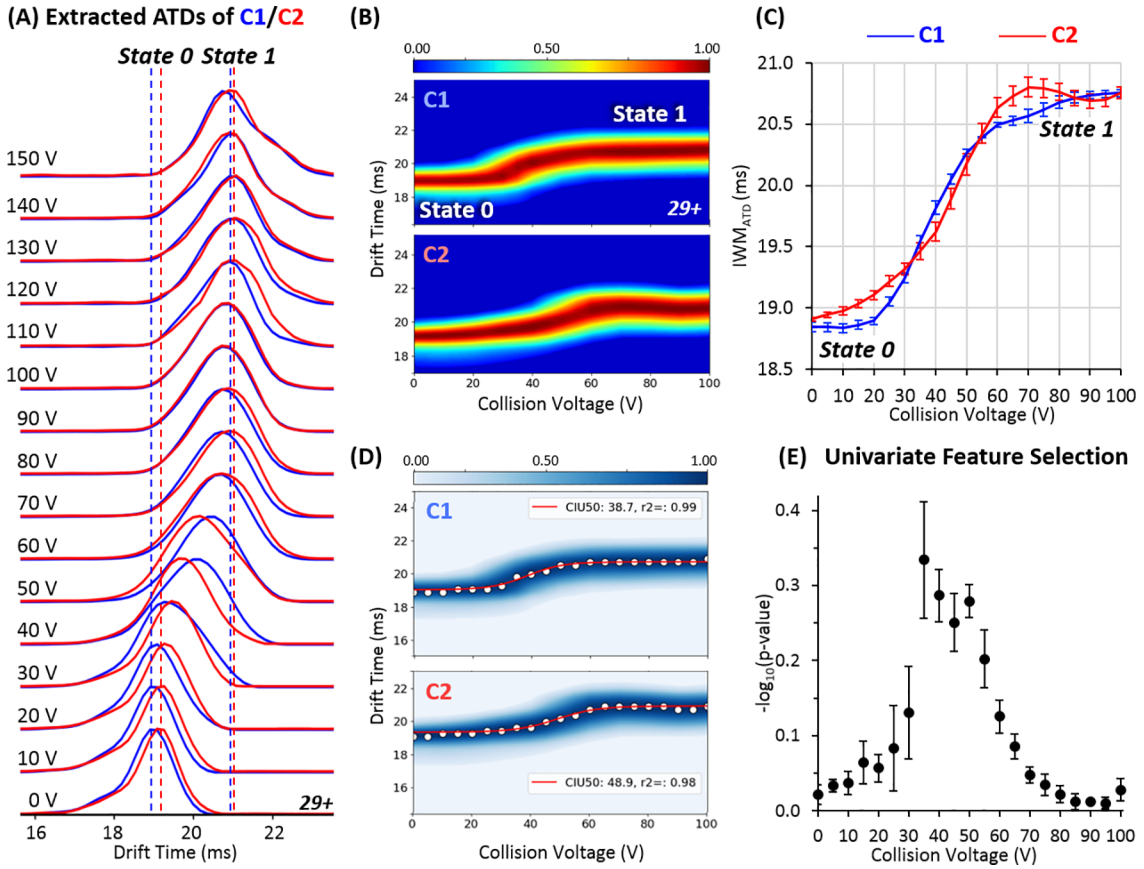

Figure 3. SEC−CIU experiments for the 29+ charge state of tsAb conformers at the intact level. (A) ATDs extracted from the respective averaged CIU plots of C1 (blue) and C2 (red). (B) CIU fingerprints. (C) Intensity weighted mean of ATDs represented as a function of CVs for both conformers. (D) Evaluation of CIU50 values. (E) Univariate feature selection plot.

states (Table S3), which is very close to the experimental error related to the IM technique. At the middle-up level, the Fab1 subunit of conformer C1 was also found to be slightly more compact ($^{TW}CCS_{N2}$ = 50.1 nm^2 for the 19+ charge state) than for conformer C2 ($^{TW}CCS_{N2}$ = 50.5 nm^2, Figure 2F). These results are in good agreement with CCS_{N2} calculated from the crystal structure of the CODV Fab1 (PDB 5WHZ).[6] The theoretical CCS_{N2} values obtained with the IMoS software was 54.8 ± 0.1 nm^2 using the EHSS method. In addition, C1 and C2 represent 18 ± 1% and 82 ± 1% of Fab1 subunits based on nIM profiles, in good agreement with SEC-UV data. Of note, only one IM population was detected for the mutant tsAb, suggesting that the two-peak elution behavior was dependent on the conformational change within the CODV Fab (Figure S2).

Overall, although slight differences are observed between the two isomers at both intact and middle-up levels, these small variations (<1%) fall within the error of IM measurement of the low resolution TWIMS platform (~2%) and thus do not allow to definitely prove the presence of two distinct conformations.

SEC−CIU Experiments to Complement Conformers' Conformational Characterization. In order to strengthen first trends from $^{TW}CCS_{N2}$ measurements on the linear TWIMS, we performed SEC−CIU on the two chromatographic peaks separated at the intact level to determine whether tsAb isomers exhibit distinct gas-phase unfolding patterns.

Extracted ATDs for the 29+ charge state show that both conformers start unfolding at the same voltage (~20 V, Figure 3A). At ~40 V, conformer C1, whose ground state (state 0) is more compact than C2, becomes more extended than C2. At ~90 V, the two species have adopted their final unfolded forms, exhibiting identical arrival times (20.8 ms) and suggesting that both conformers ultimately rearrange into the same activated state (state 1). Altogether, a single transition is detected for the two species in the 0−200 V range, which can be further visualized on CIU fingerprints (Figure 3B). As conformational differences are subtle, representing unfolding plots as intensity weighted means of each ATD (IWM_{ATD}) along the collision voltage ramp helps to better evidence small changes in average arrival times and peak width (Figure 3C). This graph, generated using Benthesikyme,[40] highlights a steep unfolding slope for C1 starting at 20 V, which indicates a transition toward a more extended conformation. Conversely, the slope remains shallower for C2 until 40 V, where a breaking point reflecting a clear conformational shift can be observed. Interestingly, C2 reaches its most extended conformation at 70 V, before C1, which was not detected on extracted ATDs. A slight recompaction of C2 is then observed at higher voltages. These differences in transitions can be further evaluated through CIU50 values, which confirm that unfolding occurs at lower collision voltage values for C1 (38.7 V) compared to C2 (48.9 V; Figure 3D). The univariate feature selection plot pinpoints the most discriminating collision voltages (~35−50 V, i.e., during conformational unfolding) between the two species (Figure 3E). Similarly,

https://doi.org/10.1021/acs.analchem.2c00928
Anal. Chem. 2022, 94, 7981−7989

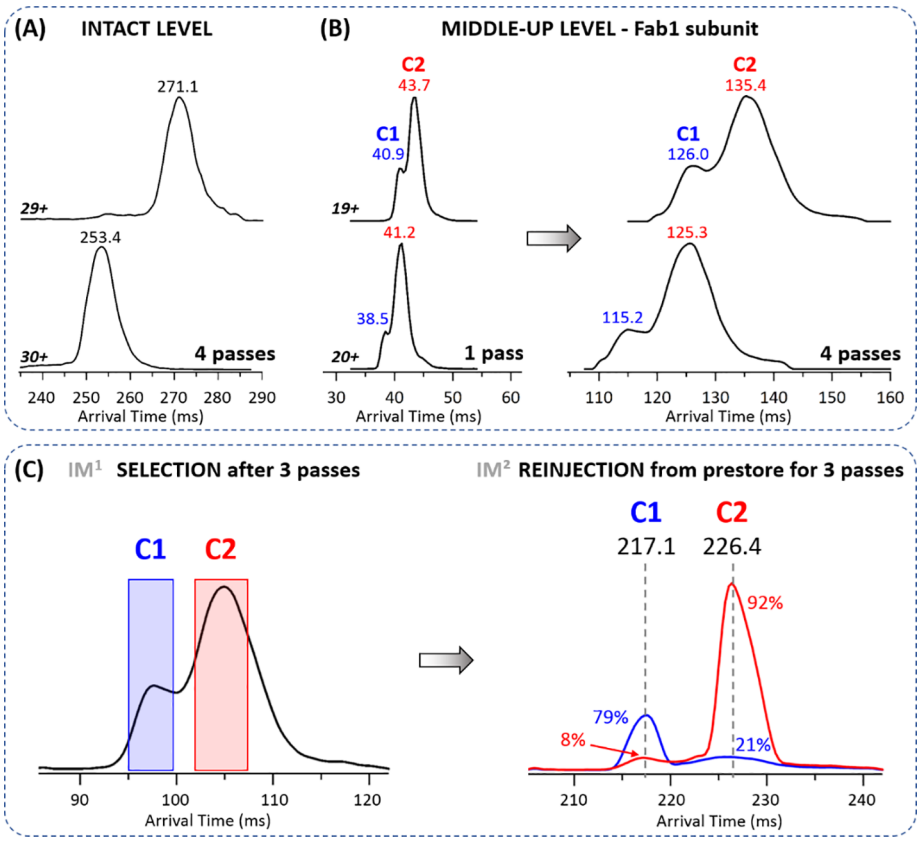

Figure 4. cIM-MS experiments. (A) Intact level analysis after four passes. ATDs were extracted for charge states 29+ and 30+. (B) Results obtained after one and four passes for the CODV Fab1 subunit. ATDs were extracted for charge states 19+ and 20+. (C) IM^2 slicing experiment performed at middle-up level, on the CODV Fab1 subunit (z = 19+). IM windows corresponding to C1 and C2 were sequentially selected, stored in the prestore, and reinjected, showing a minor isomerization between C1/C2.

distinct gas-phase conformational behaviors are obtained for the 30+ charge state, with a ΔCIU50 value of ∼10 V (Figure S3).

Altogether, SEC−CIU fingerprinting offers an additional layer of information compared to conventional SEC-(nIM-)MS experiments, showing that tsAb isomers exhibit different conformational behaviors upon gas-phase activation. These data corroborate the fact that the two peaks observed in SEC result from different conformations.

High-Resolution cIM-MS Provides Definitive Proof of the Coexistence of Two Conformers. We then moved to a cIM-MS instrument of higher IM resolution using multipass IM separation with the aim of gathering stronger evidence regarding the presence of different tsAb conformations. As the SEC coupling was not available on the cIM-MS platform at the time this work was done, the differentiation of conformers relies solely on the IM dimension. At the intact level, a single population is observed for the 29+ and 30+ charge states after four passes (Figure 4A). Because the SEC dimension is not used to provide a first separation, the IM peak of the major conformer C2 most likely overlaps the signal of the minor conformer C1, preventing the distinction of both isomers. Nonetheless, at the middle-up level, two species are clearly separated for Fab1 subunits (Figure 4B). After one pass, a difference of 2−3 ms between arrival times of C1 and C2 is obtained for both 19+ and 20+ charge states. After four passes, the separation increases to 9−10 ms (Figure 4B). Based on cIM profiles of the 19+ charge state, C1 (more compact form) and C2 (more extended form) account for 19 ± 1% and 81 ± 1% of detected Fab1 subunits, respectively, in agreement with both SEC-UV (24/76%) and SEC-nIM-MS results (18/82%) obtained on the linear TWIMS platform. These cIM-MS results (i) unequivocally confirm the coexistence of two tsAb conformers related to the Fab1 domain of the CODV arm and (ii) definitely prove that the presence of two distinct species is not an artifact of the SEC separation.

Lastly, IM^n slicing experiments were performed on the cIM-MS instrument to investigate Fab1 subunits separated at the middle-up level.[21] IM^n slicing experiments allow to isolate an ion population from the cIM cell and store it selectively for a defined amount of time before further IM analysis, affording the observation of interconversion between populations on a millisecond time scale. After three passes (IM^1), each species was sequentially sliced-out (red and blue windows in Figure 4C), stored in the prestore region, reinjected in the cIM cell for three passes, which can be summarized as IM^1 (3 passes) → Slicing → IM^2 (3 passes) (Figure S4). Two strictly identical populations at ∼217.1 and ∼226.4 ms are observed upon reinjection of each slice, meaning that only a minor interconversion between the two conformers occurs over the time scale of the cIM experiment, in line with conformational isomerization previously reported for the C1 $YP_{trans}P_{trans}$ ⇋ C2 $YP_{trans}P_{cis}$ equilibrium.[11] Overall, combining IM^n slicing with high-resolution multipass experiments of the cIM-MS instrument provide new opportunities to rapidly expose isomerization events in large biotherapeutics, which represents a major step forward compared to first-generation IM-MS instruments. Slicing IM populations is particularly interesting

https://doi.org/10.1021/acs.analchem.2c00928
Anal. Chem. 2022, 94, 7981−7989

to uncover minor isomeric forms that are not detected even with higher IM resolving powers, especially for proteins with rich conformational landscapes. In conclusion, innovative high resolution IM-MS capabilities hold a tremendous potential to develop more "IM-inclusive" analytical workflows.

CONCLUSIONS

The present study clearly shows that combining state-of-the-art IM-based approaches, such as CIU and high-resolution IM, is of utmost interest to achieve a better conformational characterization of novel mAb-based products. Here, online SEC-nMS analyses first revealed the presence of two isomers of an anti-HIV tsAb at both intact and middle-up levels, originating from two different configurations within the YPP motif of the CODV Fab subunit, which was further corroborated by the fact that only one population was observed for the intact AAP mutant. Preliminary $^{TW}CCS_{N2}$ measurements obtained with SEC-nIM-MS suggested that isomers had distinct conformations, but results remained ambiguous because $^{TW}CCS_{N2}$ variations fell within the error measurement of the low resolution TWIMS instrument. Additional SEC−CIU experiments pinpointed subtle but significant differences of gas-phase unfolding behaviors between the two intact SEC-separated species, strengthening our hypothesis regarding the coexistence of conformational isomers. Finally, the use of high-resolution cIM-MS at the middle-up level was decisive to unequivocally conclude on the coexistence of two CODV Fab conformers. Each conformer could be selected and further studied thanks to the slicing capability of the cIM-MS instrument, demonstrating a minor interconversion or isomerization between the two forms over the time scale of the cIM-MS experiment.

Overall, our results illustrate the benefits of SEC−CIU and high-resolution IM to complement more classical biophysical techniques already implemented in most R&D laboratories and, thus, improve the conformational characterization of next-generation empowered multispecific antibodies. Rapid and sensitive techniques are essential to support the ever-growing portfolio of increasingly complex biotherapeutics. Methodologies presented here address several analytical challenges to afford high-throughput online SEC-nMS analysis along with an in-depth conformational characterization of higher order structures from a multispecific antibody. The online coupling of liquid chromatography to nIM-MS is particularly well adapted to fast-paced pharmaceutical environments. In addition, we report here the first use of high-resolution cIM-MS for mAb-based products in native conditions, and envision that this instrument will undoubtedly be beneficial for biopharma companies. Indeed, multifunction capabilities of the cIM-MS instrument open new avenues to explore mobility-selected populations, also allowing to unveil isomerization events in large proteins. IM^n could be employed for rapid quantitative assessment of coexisting isomeric forms, as we have shown consistent quantitative interpretation based on SEC-UV, SEC-nIM-MS and cIM profiles. The described IM-based methodologies could be used to solve such challenges and extended to a large variety of complex antibody constructs generating isomers, and could even be extended to the study of mAb and antigen binding stoichiometry. There is a strong need to tackle analytical challenges driven by mAb conformers since protein engineering intended to fix isomerization may not be an option as it would significantly impact antigen binding, and so we believe that high-resolution IM/CIU approaches, coupled to SEC for fast efficient desalting, have the potential to integrate the analytical toolbox of biopharma for the development of next-generation antibody products.

ASSOCIATED CONTENT

Supporting Information

The Supporting Information is available free of charge at https://pubs.acs.org/doi/10.1021/acs.analchem.2c00928.

Voltages used to set the direction of the ions in the multifunction array region of cIM-MS spectrometer for each type of cIM event (Table S1); Comparison of theoretical and experimental masses obtained by SEC-nMS (Table S2); $^{TW}CCS_{N2}$ measurements for the two tsAb conformers at intact and middle-up levels (Table S3); Evaluation of secondary interactions occurring with the SEC stationary phase (Figure S1); Analysis of mutant tsAb using online SEC-nMS/nIM-MS (Figure S2); SEC−CIU experiments for the 30+ charge state of intact tsAb conformers (Figure S3); Principle of IM^n slicing on the cIM-MS instrument (Figure S4) (PDF)

AUTHOR INFORMATION

Corresponding Author

Sarah Cianférani − *Laboratoire de Spectrométrie de Masse BioOrganique, Université de Strasbourg, CNRS, IPHC UMR 7178, 67087 Strasbourg, France; Infrastructure Nationale de Protéomique ProFI − FR2048, 67087 Strasbourg, France;* orcid.org/0000-0003-4013-4129; Email: sarah.cianferani@unistra.fr

Authors

Evolène Deslignière − *Laboratoire de Spectrométrie de Masse BioOrganique, Université de Strasbourg, CNRS, IPHC UMR 7178, 67087 Strasbourg, France; Infrastructure Nationale de Protéomique ProFI − FR2048, 67087 Strasbourg, France*

Simon Ollivier − *INRAE, UR BIA, F-44316 Nantes, France; INRAE, BIBS Facility, F-44316 Nantes, France;* orcid.org/0000-0002-7671-1736

Anthony Ehkirch − *Laboratoire de Spectrométrie de Masse BioOrganique, Université de Strasbourg, CNRS, IPHC UMR 7178, 67087 Strasbourg, France; Infrastructure Nationale de Protéomique ProFI − FR2048, 67087 Strasbourg, France*

Armelle Martelet − *CMC Development, BioAnalytics department France, SANOFI R&D, 94400 Vitry-sur-Seine, France*

David Ropartz − *INRAE, UR BIA, F-44316 Nantes, France; INRAE, BIBS Facility, F-44316 Nantes, France;* orcid.org/0000-0003-4767-6940

Nelly Lechat − *CMC Development, BioAnalytics department France, SANOFI R&D, 94400 Vitry-sur-Seine, France*

Oscar Hernandez-Alba − *Laboratoire de Spectrométrie de Masse BioOrganique, Université de Strasbourg, CNRS, IPHC UMR 7178, 67087 Strasbourg, France; Infrastructure Nationale de Protéomique ProFI − FR2048, 67087 Strasbourg, France*

Jean-Michel Menet − *CMC Development, BioAnalytics department France, SANOFI R&D, 94400 Vitry-sur-Seine, France*

Séverine Clavier − *CMC Development, BioAnalytics department France, SANOFI R&D, 94400 Vitry-sur-Seine, France*

https://doi.org/10.1021/acs.analchem.2c00928
Anal. Chem. 2022, 94, 7981−7989

Hélène Rogniaux − *INRAE, UR BIA, F-44316 Nantes, France; INRAE, BIBS Facility, F-44316 Nantes, France;* orcid.org/0000-0001-6083-2034

Bruno Genet − *CMC Development, BioAnalytics department France, SANOFI R&D, 94400 Vitry-sur-Seine, France*

Complete contact information is available at: https://pubs.acs.org/10.1021/acs.analchem.2c00928

Author Contributions

The manuscript was written through contributions of all authors. All authors have given approval to the final version of the manuscript.

Notes

The authors declare no competing financial interest.

■ ACKNOWLEDGMENTS

This work was supported by the CNRS, the University of Strasbourg, the "Agence Nationale de la Recherche" and the French Proteomic Infrastructure (ProFI; ANR-10-INBS-08-03). The authors would like to thank GIS IBiSA and Région Grand Est for financial support in purchasing a Synapt G2 HDMS instrument, as well as GIS IBiSA, Nantes Métropole, Région Pays de la Loire and FEDER for financial support in purchasing a SELECT SERIES Cyclic IMS instrument. E.D. and A.E. acknowledge the French Ministry for Education and Research, and the "Association Nationale de la Recherche et de la Technologie" (ANRT) and Syndivia, respectively, for funding of their Ph.D. S.O. acknowledges the "Agence Nationale de la Recherche" (Grant ANR-18-CE29-0006) for funding of his Ph.D. The authors would like to thank Alessandro Masiero and Paul Ferrari's team (Biologics research France, E-Biology, SANOFI R&D, France) for the engineering and production of the mutant antibody. The authors gratefully acknowledge Laurent Duhau and Stéphane Cornen (CMC Development, SANOFI R&D, France) for their support.

■ REFERENCES

(1) Husain, B.; Ellerman, D. *BioDrugs* **2018**, *32* (5), 441−464.
(2) Mullard, A. *Nat. Rev. Drug Discovery* **2021**, *20* (7), 491−495.
(3) Spiess, C.; Zhai, Q.; Carter, P. J. *Mol. Immunol* **2015**, *67* (2), 95−106.
(4) Kontermann, R. E.; Brinkmann, U. *Drug Discovery Today* **2015**, *20* (7), 838−847.
(5) Brinkmann, U.; Kontermann, R. E. *mAbs* **2017**, *9* (2), 182−212.
(6) Xu, L.; Pegu, A.; Rao, E.; Doria-Rose, N.; Beninga, J.; McKee, K.; Lord, D. M.; Wei, R. R.; Deng, G.; Louder, M.; Schmidt, S. D.; Mankoff, Z.; Wu, L.; Asokan, M.; Beil, C.; Lange, C.; Leuschner, W. D.; Kruip, J.; Sendak, R.; Do Kwon, Y.; Zhou, T.; Chen, X.; Bailer, R. T.; Wang, K.; Choe, M.; Tartaglia, L. J.; Barouch, D. H.; O'Dell, S.; Todd, J.-P.; Burton, D. R.; Roederer, M.; Connors, M.; Koup, R. A.; Kwong, P. D.; Yang, Z.-y.; Mascola, J. R.; Nabel, G. J. *Science* **2017**, *358* (6359), 85−90.
(7) Wu, X.; Yang, Z.-Y.; Li, Y.; Hogerkorp, C.-M.; Schief, W. R.; Seaman, M. S.; Zhou, T.; Schmidt, S. D.; Wu, L.; Xu, L.; Longo, N. S.; McKee, K.; O'Dell, S.; Louder, M. K.; Wycuff, D. L.; Feng, Y.; Nason, M.; Doria-Rose, N.; Connors, M.; Kwong, P. D.; Roederer, M.; Wyatt, R. T.; Nabel, G. J.; Mascola, J. R. *Science* **2010**, *329* (5993), 856−861.
(8) Pegu, A.; Yang, Z.-y.; Boyington, J. C.; Wu, L.; Ko, S.-Y.; Schmidt, S. D.; McKee, K.; Kong, W.-P.; Shi, W.; Chen, X.; Todd, J.-P.; Letvin, N. L.; Huang, J.; Nason, M. C.; Hoxie, J. A.; Kwong, P. D.; Connors, M.; Rao, S. S.; Mascola, J. R.; Nabel, G. J. *Science Translational Medicine* **2014**, *6* (243), na.
(9) Sok, D.; van Gils, M. J.; Pauthner, M.; Julien, J.-P.; Saye-Francisco, K. L.; Hsueh, J.; Briney, B.; Lee, J. H.; Le, K. M.; Lee, P. S.; Hua, Y.; Seaman, M. S.; Moore, J. P.; Ward, A. B.; Wilson, I. A.; Sanders, R. W.; Burton, D. R. *Proc. Natl. Acad. Sci. U. S. A.* **2014**, *111* (49), 17624−17629.
(10) Kwon, Y. D.; Georgiev, I. S.; Ofek, G.; Zhang, B.; Asokan, M.; Bailer, R. T.; Bao, A.; Caruso, W.; Chen, X.; Choe, M.; Druz, A.; Ko, S.-Y.; Louder, M. K.; McKee, K.; O'Dell, S.; Pegu, A.; Rudicell, R. S.; Shi, W.; Wang, K.; Yang, Y.; Alger, M.; Bender, M. F.; Carlton, K.; Cooper, J. W.; Blinn, J.; Eudailey, J.; Lloyd, K.; Parks, R.; Alam, S. M.; Haynes, B. F.; Padte, N. N.; Yu, J.; Ho, D. D.; Huang, J.; Connors, M.; Schwartz, R. M.; Mascola, J. R.; Kwong, P. D.; Sundquist, W. I. *J. Virol* **2016**, *90* (13), 5899−5914.
(11) Masiero, A.; Lechat, N.; Gentric, M.; Sourrouille, C.; Laville, F.; Crépin, R.; Borel, C.; Ziegler, C.; Bisch, G.; Leclerc, E.; Laurent, L.; Brault, D.; Alexandre, S.; Gagnaire, M.; Duffieux, F.; Soubrier, F.; Capdevila, C.; Arnould, I.; Dumas, J.; Dabin, J.; Genet, B.; Radošević, K.; Menet, J.-M.; Prades, C. *mAbs* **2020**, *12* (1), 1698128.
(12) Shinoda, K.; Fujitani, H. *Sci. Rep* **2017**, *7* (1), na.
(13) Joseph, A. P.; Srinivasan, N.; de Brevern, A. G. *Amino Acids* **2012**, *43* (3), 1369−1381.
(14) Guttman, M.; Padte, N. N.; Huang, Y.; Yu, J.; Rocklin, G. J.; Weitzner, B. D.; Scian, M.; Ho, D. D.; Lee, K. K. *Sci. Rep* **2020**, *10* (1), na.
(15) Ehkirch, A.; Hernandez-Alba, O.; Colas, O.; Beck, A.; Guillarme, D.; Cianferani, S. *J. Chromatogr B: Anal Technol. Biomed Life Sci.* **2018**, *1086*, 176−183.
(16) Füssl, F.; Strasser, L.; Carillo, S.; Bones, J. *Curr. Opin Biotechnol* **2021**, *71*, 32−40.
(17) Murisier, A.; Duivelshof, B. L.; Fekete, S.; Bourquin, J.; Schmudlach, A.; Lauber, M. A.; Nguyen, J. M.; Beck, A.; Guillarme, D.; D'Atri, V. *J. Chromatogr A* **2021**, *1655*, 462499.
(18) Botzanowski, T.; Hernandez-Alba, O.; Malissard, M.; Wagner-Rousset, E.; Deslignière, E.; Colas, O.; Haeuw, J.-F.; Beck, A.; Cianférani, S. *Anal. Chem.* **2020**, *92* (13), 8827−8835.
(19) Hernandez-Alba, O.; Wagner-Rousset, E.; Beck, A.; Cianferani, S. *Anal. Chem.* **2018**, *90* (15), 8865−8872.
(20) Deng, L.; Webb, I. K.; Garimella, S. V. B.; Hamid, A. M.; Zheng, X.; Norheim, R. V.; Prost, S. A.; Anderson, G. A.; Sandoval, J. A.; Baker, E. S.; Ibrahim, Y. M.; Smith, R. D. *Anal. Chem.* **2017**, *89* (8), 4628−4634.
(21) Giles, K.; Ujma, J.; Wildgoose, J.; Pringle, S.; Richardson, K.; Langridge, D.; Green, M. *Anal. Chem.* **2019**, *91* (13), 8564−8573.
(22) Kenderdine, T.; Nemati, R.; Baker, A.; Palmer, M.; Ujma, J.; FitzGibbon, M.; Deng, L.; Royzen, M.; Langridge, J.; Fabris, D. *J. Mass Spectrom* **2020**, *55* (2), 4465−4476.
(23) McKenna, K. R.; Li, L.; Baker, A. G.; Ujma, J.; Krishnamurthy, R.; Liotta, C. L.; Fernandez, F. M. *Analyst* **2019**, *144* (24), 7220−7226.
(24) Eldrid, C.; Ujma, J.; Kalfas, S.; Tomczyk, N.; Giles, K.; Morris, M.; Thalassinos, K. *Anal. Chem.* **2019**, *91* (12), 7554−7561.
(25) Eldrid, C.; Ben-Younis, A.; Ujma, J.; Britt, H.; Cragnolini, T.; Kalfas, S.; Cooper-Shepherd, D.; Tomczyk, N.; Giles, K.; Morris, M.; Akter, R.; Raleigh, D.; Thalassinos, K. *J. Am. Soc. Mass Spectrom.* **2021**, *32* (6), 1545−1552.
(26) Snyder, D. T.; Jones, B. J.; Lin, Y.-F.; Cooper-Shepherd, D. A.; Hewitt, D.; Wildgoose, J.; Brown, J. M.; Langridge, J. I.; Wysocki, V. H. *Analyst* **2021**, *146* (22), 6861−6873.
(27) Tian, Y.; Han, L.; Buckner, A. C.; Ruotolo, B. T. *Anal. Chem.* **2015**, *87* (22), 11509−11515.
(28) Botzanowski, T.; Erb, S.; Hernandez-Alba, O.; Ehkirch, A.; Colas, O.; Wagner-Rousset, E.; Rabuka, D.; Beck, A.; Drake, P. M.; Cianferani, S. *mAbs* **2017**, *9* (5), 801−811.
(29) Desligniere, E.; Ehkirch, A.; Duivelshof, B. L.; Toftevall, H.; Sjogren, J.; Guillarme, D.; D'Atri, V.; Beck, A.; Hernandez-Alba, O.; Cianferani, S. *Pharmaceuticals (Basel)* **2021**, *14* (6), 498.
(30) Watanabe, Y.; Vasiljevic, S.; Allen, J. D.; Seabright, G. E.; Duyvesteyn, H. M. E.; Doores, K. J.; Crispin, M.; Struwe, W. B. *Anal. Chem.* **2018**, *90* (12), 7325−7331.
(31) Deslignière, E.; Ehkirch, A.; Botzanowski, T.; Beck, A.; Hernandez-Alba, O.; Cianférani, S. *Anal. Chem.* **2020**, *92* (19), 12900−12908.

(32) Lermyte, F.; Tsybin, Y. O.; O'Connor, P. B.; Loo, J. A. *J. Am. Soc. Mass Spectrom.* **2019**, *30* (7), 1149−1157.
(33) Debaene, F.; Boeuf, A.; Wagner-Rousset, E.; Colas, O.; Ayoub, D.; Corvaia, N.; Van Dorsselaer, A.; Beck, A.; Cianferani, S. *Anal. Chem.* **2014**, *86* (21), 10674−83.
(34) Marcoux, J.; Champion, T.; Colas, O.; Wagner-Rousset, E.; Corvaia, N.; Van Dorsselaer, A.; Beck, A.; Cianferani, S. *Protein Sci.* **2015**, *24* (8), 1210−23.
(35) Bush, M. F.; Hall, Z.; Giles, K.; Hoyes, J.; Robinson, C. V.; Ruotolo, B. T. *Anal. Chem.* **2010**, *82* (22), 9557−65.
(36) Shrivastav, V.; Nahin, M.; Hogan, C. J.; Larriba-Andaluz, C. *J. Am. Soc. Mass Spectrom.* **2017**, *28* (8), 1540−1551.
(37) Marklund, E. G.; Degiacomi, M. T.; Robinson, C. V.; Baldwin, A. J.; Benesch, J. L. P. *Structure* **2015**, *23* (4), 791−799.
(38) Polasky, D. A.; Dixit, S. M.; Fantin, S. M.; Ruotolo, B. T. *Anal. Chem.* **2019**, *91* (4), 3147−3155.
(39) Migas, L. G.; France, A. P.; Bellina, B.; Barran, P. E. *Int. J. Mass Spectrom.* **2018**, *427*, 20−28.
(40) Sivalingam, G. N.; Cryar, A.; Williams, M. A.; Gooptu, B.; Thalassinos, K. *Int. J. Mass Spectrom.* **2018**, *426*, 29−37.
(41) Arakawa, T.; Ejima, D.; Li, T.; Philo, J. S. *J. Pharm. Sci.* **2010**, *99* (4), 1674−1692.

https://doi.org/10.1021/acs.analchem.2c00928
Anal. Chem. 2022, 94, 7981−7989